JOURNAL OF COMPUTATIONAL PHYSICS 73, 267–288 (1987)

Flame Sheet Starting Estimates for Counterflow Diffusion Flame Problems*

D. E. KEYES AND M. D. SMOOKE

Department of Mechanical Engineering, Yale University, New Haven, Connecticut 06520

Received March 14, 1986; revised October 29, 1986

We develop a flame sheet starting procedure for the detailed numerical modeling of counterflow diffusion flames. These flames are characterized by the presence of a narrow reaction zone stabilized between counterflowing jets of fuel and oxidizer. Despite the outwardly simple form of the governing equations, the determination of a good initial solution estimate can be difficult. Failure to obtain such an approximation can cause the numerical solution procedure to converge slowly or to diverge. The flame sheet model we consider couples the conservation of mass and momentum with a Shvab–Zeldovich equation to provide starting estimates for the mass flux in the transverse direction, the similarity function, the temperature, and the stable major species in the flame. Application of the model to two methane–air flames reveals the effectiveness of the procedure in generating starting estimates for such problems.

1. INTRODUCTION

Results obtained from the solution of counterflow diffusion flames have been used by combustion scientists in the investigation of chemically controlled extinction limits, in the characterization of the combustion processes occurring in turbulent flames, and in the study of pollutant formation (see, e.g., [1]). Experimentally these flames can be produced when a reaction zone is stabilized near the stagnation point of two infinitely wide coaxial concentric jets [2] (see Fig. 1). Fuel is emitted from one jet and oxidizer (air) from the other. In addition to the double-jet configuration, Tsuji and Yamaoka have investigated counterflow diffusion flames in which fuel is emitted from a porous cylinder into an oncoming stream of air (see Fig. 2) [3–5]. A free stagnation line parallel to the cylinder axis forms in front of the cylinder's porous surface. In both cases, combustion occurs within a thin flame zone near the stagnation point (line) where the fuel and the oxidizer are in stoichiometric proportion. The modeling of both experimental configurations can be reduced to the solution of a system of coupled nonlinear two-point boundary value problems along the stagnation point streamline. Despite the outwardly simple form of these problems, the determination of a "good" initial solution estimate can be difficult. The difficulty is due to the exponential depen-

* Work supported by the Office of Naval Research.

0021-9991/87 $3.00

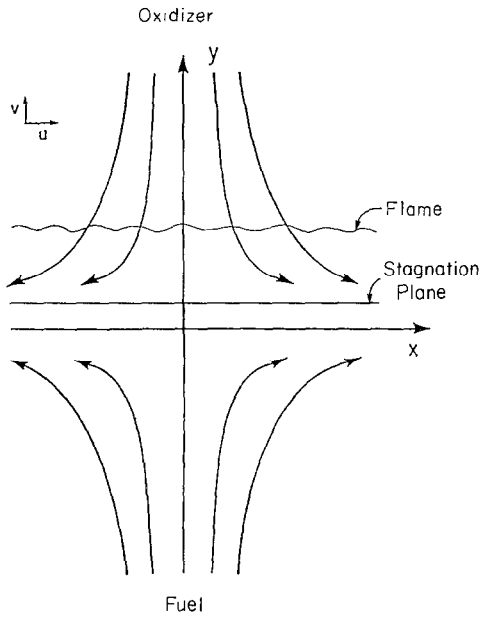

FIG. 1. Schematic of the double-jet (Seshadri) counterflow diffusion flame.

dence of the chemistry terms on the temperature and to the nonlinear coupling of the fluid and the thermochemistry solution fields.

In previous work, we focused our efforts on the solution of adiabatic and non-adiabatic premixed laminar flames by adaptive finite difference methods [6–7]. In these problems the governing differential equations were discretized and the resulting nonlinear difference equations were solved by Newton's method. Cubic polynomials and Gaussian shaped profiles were used as starting estimates for the major and minor species on an initial coarse grid. In addition, the energy equation was replaced by a fixed (e.g., experimental) temperature profile and a time-depen-

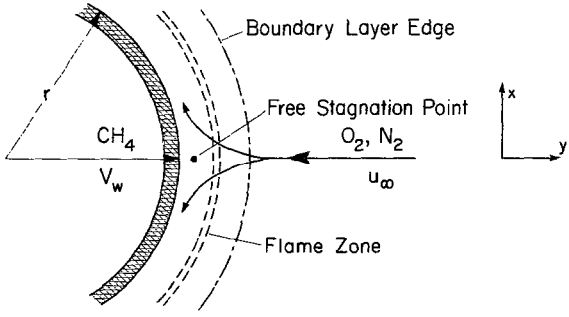

FIG. 2. Schematic of the porous cylinder (Tsuji) counterflow diffusion flame.

dent integration algorithm was used to help bring the starting estimates into the domain of convergence of Newton's method. The species solution was then used as a starting estimate for the full energy–species system. The combination of these procedures reduced significantly the convergence difficulties that were obtained when the full energy–species system was solved initially on a fine grid.

In adiabatic and nonadiabatic premixed laminar flame problems the conservation of mass and momentum reduces to the specification of a constant mass flow rate and a constant thermodynamic pressure [6–7]. Hence, thermochemical considerations play a more important role in these problems than do fluid dynamical aspects. This is not the case in counterflow diffusion flames. There is a strong coupling between the fluid dynamic and the thermochemistry solution fields in these flames. We have found that, although the solution procedure used in premixed laminar flame problems can work in selected counterflow cases, it does not provide a sufficiently robust or efficient starting estimate from which Newton's method will converge. In addition, the relaxation to steady-state (or at least until the solution is within the convergence domain of Newton's method) is very slow. The importance of these flames in modeling turbulent reacting flows and in the determination of chemically controlled extinction limits, however, necessitates the development of an efficient starting procedure. In this paper we couple the appropriate equations of mass and momentum with a Shvab–Zeldovich equation to provide flame sheet starting estimates for the mass flux in the transverse direction, the similarity function, the temperature, and the stable major species in the flame.

In the next section we review briefly the counterflow diffusion flame model and in Section 3 we develop the flame sheet starting estimate. The model is applied to two methane–air counterflow diffusion flames in Section 4.

2. Problem Formulation

Our model for counterflow diffusion flames assumes a laminar, stagnation point flow. Hence, the governing boundary layer equations for mass, momentum, chemical species, and energy can be written in the form

$$\frac{\partial(\rho u x^{\alpha})}{\partial x} + \frac{\partial(\rho v x^{\alpha})}{\partial y} = 0, \tag{2.1}$$

$$\rho u \frac{\partial u}{\partial x} + \rho v \frac{\partial u}{\partial y} + \frac{\partial p}{\partial x} - \frac{\partial}{\partial y}\left(\mu \frac{\partial u}{\partial y}\right) = 0, \tag{2.2}$$

$$\rho u \frac{\partial Y_k}{\partial x} + \rho v \frac{\partial Y_k}{\partial y} + \frac{\partial}{\partial y}(\rho Y_k V_{ky}) - \dot{w}_k W_k = 0, \qquad k = 1, 2, ..., K, \tag{2.3}$$

$$\rho u c_p \frac{\partial T}{\partial x} + \rho v c_p \frac{\partial T}{\partial y} - \frac{\partial}{\partial y}\left(\lambda \frac{\partial T}{\partial y}\right) + \sum_{k=1}^{K} \rho Y_k V_{ky} c_{pk} \frac{\partial T}{\partial y} + \sum_{k=1}^{K} \dot{w}_k W_k h_k = 0, \tag{2.4}$$

where α represents a geometric factor ($\alpha = 0$ for cartesian coordinates and $\alpha = 1$ for cylindrical coordinates). The system is closed with the ideal gas law,

$$\rho = p\bar{W}/RT. \tag{2.5}$$

In these equations, x and y denote independent spatial coordinates in the tangential and transverse directions, respectively; T, the temperature; Y_k, the mass fraction of the kth species; p, the pressure; u and v, the tangential and the transverse components of the velocity, respectively; ρ, the mass density; W_k, the molecular weight of the kth species; $\bar{W}$, the mean molecular weight of the mixture; R, the universal gas constant; λ, the thermal conductivity of the mixture; c_p, the constant pressure heat capacity of the mixture; c_{pk}, the constant pressure heat capacity of the kth species; $\dot{w}_k$, the molar rate of production of the kth species per unit volume; h_k, the specific enthalpy of the kth species; μ the viscosity of the mixture; and V_{ky} is the diffusion velocity of the kth species in the y direction. In both configurations the free stream (tangential) velocity at the edge of the boundary layer is given by $u_\infty = ax$, where a is the strain rate.

We introduce the notation

$$f' = u/u_\infty, \tag{2.6}$$

$$V = \rho v, \tag{2.7}$$

where f' is related to the derivative of a modified stream function (see, e.g., Dixon-Lewis *et al.* [8]). Using these expressions, the boundary layer equations can be transformed into a system of ordinary differential equations valid along the stagnation-point streamline $x = 0$. For a system in rectangular or cylindrical coordinates, we have

$$\frac{dV}{dy} + a(1+\alpha)\rho f' = 0, \tag{2.8}$$

$$\frac{d}{dy}\left(\mu \frac{df'}{dy}\right) - V\frac{df'}{dy} + a(\rho_\infty - \rho(f')^2) = 0, \tag{2.9}$$

$$-\frac{d}{dy}(\rho Y_k V_k) - V\frac{dY_k}{dy} + \dot{w}_k W_k = 0, \qquad k = 1, 2, ..., K, \tag{2.10}$$

$$\frac{d}{dy}\left(\lambda \frac{dT}{dy}\right) - c_p V \frac{dT}{dy} - \sum_{k=1}^{K} \rho Y_k V_k c_{pk} \frac{dT}{dy} - \sum_{k=1}^{K} \dot{w}_k W_k h_k = 0. \tag{2.11}$$

The boundary conditions for the double-jet configuration at $y = -\infty$ are given by

$$V = V_{-\infty}, \tag{2.12}$$

$$f' = \sqrt{\rho_\infty / \rho_{-\infty}}, \tag{2.13}$$

$$Y_k = Y_{k_{-\infty}}, \qquad k = 1, 2, ..., K, \tag{2.14}$$

$$T = T_{-\infty}, \tag{2.15}$$

and at $y = \infty$ by

$$f' = 1, \tag{2.16}$$

$$Y_k = Y_{k_\infty}, \qquad k = 1, 2, ..., K, \tag{2.17}$$

$$T = T_\infty. \tag{2.18}$$

The mass flux, temperature, and species mass fractions ($V_{-\infty}$, $T_{-\infty}$, $Y_{k_{-\infty}}$) in the fuel jet are specified quantities, as are the temperature and species mass fractions (T_∞ and Y_{k_∞}) in the oxidizer jet.

At the cylinder wall $y = 0$ in the Tsuji configuration, we have

$$V(0) = V_w, \tag{2.19}$$

$$f'(0) = 0, \tag{2.20}$$

$$Y_k(0) + \frac{\rho Y_k(0) V_k}{V_w} = \varepsilon_k, \qquad k = 1, 2, ..., K, \tag{2.21}$$

$$T(0) = T_w, \tag{2.22}$$

and at $y = \infty$,

$$f' = 1, \tag{2.23}$$

$$Y_k = Y_{k_\infty}, \qquad k = 1, 2, ..., K, \tag{2.24}$$

$$T = T_\infty. \tag{2.25}$$

The mass flux, temperature, and the incoming mass flux fractions (V_w, T_w, and ε_k) at the wall are specified, as are the mass fractions of the species and the temperature (Y_{k_∞} and T_∞) at the edge of the boundary layer. The form of the chemical production rates and the expressions used in evaluating the diffusion velocities can be found in detail in Kee *et al.* [9–10].

3. Flame Sheet Model

The burning rate in a diffusion flame is controlled by the rate at which the fuel and the oxidizer are brought together in the proper proportions. This is in contrast to premixed flames where the burning rate is controlled by chemical reactions. In

the limit of infinitely fast kinetics, the fuel and the oxidizer are separated by a thin exothermic reaction zone. In this zone the fuel and the oxidizer are in stoichiometric proportion and the temperature and products of combustion are maximized. In such an ideal situation, no oxidizer is present on the fuel side and no fuel is present on the oxidizer side. The fuel and oxidizer diffuse towards the reaction zone as a result of concentration gradients in the flow. In diffusion flames of practical interest, the oxidation of the fuel to form intermediates and products proceeds through a detailed kinetics mechanism (see, e.g., [11–12]). In these problems combustion takes place at a finite rate and some fuel and oxidizer co-exist on either side of the reaction zone. Nevertheless, the use of an infinitely fast, thin flame global reaction model is a natural starting point for the determination of a "good" initial solution estimate for the finite rate counterflow model. The thin flame approximation has a long and useful history in combustion literature [13], and similar ideas have been used by Smith *et al.* [14] in the solution of premixed flames in a stagnation point flow and by Mitchell [15] (see also [16]) in the solution of axisymmetric laminar diffusion flames. This contribution seeks to revive interest in the flame sheet as an intermediate computational step in more complex problems. Because of our limited objective for the model, our assumptions below are not the most general possible (see [17] for a systematic derivation).

Our starting point is the assumption that the fuel and the oxidizer obey a single overall irreversible reaction of the type

$$\text{Fuel}(F) + \text{Oxidizer}(O) \rightarrow \text{Products}(P), \tag{3.1}$$

in the presence of an inert gas (N). We have

$$\nu_F F + \nu_O O \rightarrow \nu_P P, \tag{3.2}$$

where ν_F, ν_O, ν_P are the stoichiometric coefficients of the fuel, the oxidizer, and the product, respectively. In addition, we neglect thermal diffusion and assume that the ordinary mass diffusion velocities can be written in terms of Fick's law, i.e.,

$$V_k = -\frac{D_k}{Y_k}\frac{dY_k}{dy}, \qquad k = 1, 2, ..., K, \tag{3.3}$$

where D_k is the diffusion coefficient of the kth species with respect to the mixture. We also take $c_{pk} = c_p$ to be a constant independent of temperature. With these approximations we can write

$$\frac{dV}{dy} + a(1+\alpha)\,\rho f' = 0, \tag{3.4}$$

$$\frac{d}{dy}\left(\mu\frac{df'}{dy}\right) - V\frac{df'}{dy} + a(\rho_\infty - \rho(f')^2) = 0, \tag{3.5}$$

$$\frac{d}{dy}\left(\rho D_F\frac{dY_F}{dy}\right) - V\frac{dY_F}{dy} - W_F\nu_F\dot{w} = 0, \tag{3.6}$$

$$\frac{d}{dy}\left(\rho D_O \frac{dY_O}{dy}\right) - V\frac{dY_O}{dy} - W_O v_O \dot{w} = 0, \tag{3.7}$$

$$\frac{d}{dy}\left(\rho D_P \frac{dY_P}{dy}\right) - V\frac{dY_P}{dy} + W_P v_P \dot{w} = 0, \tag{3.8}$$

$$\frac{d}{dy}\left(\rho D_N \frac{dY_N}{dy}\right) - V\frac{dY_N}{dy} = 0, \tag{3.9}$$

$$\frac{d}{dy}\left(\frac{\lambda}{c_p}\frac{dT}{dy}\right) - V\frac{dT}{dy} + \frac{(W_F v_F h_F + W_O v_O h_O - W_P v_P h_P)}{c_p}\dot{w} = 0, \tag{3.10}$$

where

$$\dot{w} = -\frac{\dot{w}_F}{v_F} = -\frac{\dot{w}_O}{v_0} = \frac{\dot{w}_P}{v_P}, \tag{3.11}$$

is the rate of progress of the reaction and where we have made use of the fact that $\sum_{k=1}^{K} Y_k V_k = 0$.

If we introduce the heat release per unit mass of the fuel Q, where

$$Q = h_F + \frac{W_O v_O}{W_F v_F} h_O - \frac{W_P v_P}{W_F v_F} h_P, \tag{3.12}$$

and if we assume that the Lewis numbers

$$\mathrm{Le}_F = \frac{\lambda}{\rho D_F c_p}, \qquad \mathrm{Le}_O = \frac{\lambda}{\rho D_O c_p}, \tag{3.13a}$$

$$\mathrm{Le}_P = \frac{\lambda}{\rho D_P c_p}, \qquad \mathrm{Le}_N = \frac{\lambda}{\rho D_N c_p}, \tag{3.13b}$$

are all equal to one (i.e., the D_k are all equal to a common $D = \lambda/\rho c_p$), then each of the Shvab–Zeldovich coupling functions

$$Z_F = Y_F - Y_{F_\infty} + \frac{c_p}{Q}(T - T_\infty), \tag{3.14}$$

$$Z_0 = Y_0 - Y_{0_\infty} + \frac{c_p}{Q}\frac{W_O v_O}{W_F v_F}(T - T_\infty), \tag{3.15}$$

$$Z_P = Y_P - Y_{P_\infty} - \frac{c_p}{Q}\frac{W_P v_P}{W_F v_F}(T - T_\infty), \tag{3.16}$$

$$Z_N = Y_N - Y_{N_\infty}, \tag{3.17}$$

satisfies the differential equation

$$\frac{d}{dy}\left(\rho D \frac{dZ_k}{dy}\right) - V\frac{dZ_k}{dy} = 0, \qquad k = F, O, P, N, \tag{3.18}$$

with

$$Z_k(-\infty) = Z_{k_{-\infty}}, \tag{3.19}$$

$$Z_k(\infty) = 0, \tag{3.20}$$

for the double-jet problem and

$$Z_k(0) - \frac{\rho D}{V_w}\frac{dZ_k(0)}{dy} = Z_{k_w}, \tag{3.21}$$

$$Z_k(\infty) = 0, \tag{3.22}$$

for the Tsuji configuration. In both cases $Z_{k_{-\infty}}$ and Z_{k_w} are constant. (Strictly, the derivation of (3.21) depends on a mixed condition on T at the burner, as opposed to the experimentally available Dirichlet form (2.22).) As a result, all of the Z_k are proportional to each other and to the conserved scalar S which, for the double-jet problem, satisfies

$$\frac{d}{dy}\left(\rho D \frac{dS}{dy}\right) - V\frac{dS}{dy} = 0, \tag{3.23}$$

$$S(-\infty) = 1, \tag{3.24}$$

$$S(\infty) = 0. \tag{3.25}$$

The flame sheet model can be developed for both experimental configurations. For convenience, in the discussion that follows, we continue our development for the double jet.

From (3.18)–(3.20) and (3.23)–(3.25) we can write

$$Z_k = Z_{k_{-\infty}} S(y), \qquad k = F, O, P, N. \tag{3.26}$$

Equation (3.23) can be coupled with Eq. (3.4) and (3.5) to obtain profiles for V, f', and S. To complete the specification of the starting estimate, we must be able to recover the temperature and the major species profiles from the conserved scalar. Of critical importance to this procedure is an estimate of the location of the flame front, y_f.

In the Shvab–Zeldovich formulation, fuel and oxidizer cannot co-exist. Hence, on the fuel side of the flame $Y_O = 0$ and on the oxidizer side $Y_F = 0$. If we denote variables at the flame front with the subscript f, then from (3.26) we can write

$$Z_{F_f} = \frac{Z_{F_{-\infty}}}{Z_{O_{-\infty}}} Z_{O_f}, \tag{3.27}$$

and with $Y_{F_f} = Y_{O_f} = Y_{F_\infty} = 0$ and (3.14)–(3.15) we have

$$Z_{F_f} = -\frac{Z_{F_{-\infty}} Y_{O_\infty}}{Z_{O_{-\infty}}} \frac{1}{1 - \dfrac{Z_{F_{-\infty}}}{Z_{O_{-\infty}}} \dfrac{W_O \nu_O}{W_F \nu_F}}. \tag{3.28}$$

If we use (3.28) in the relation $S(y_f) = Z_{F_f}/Z_{F_{-\infty}}$, we can obtain a value for the conserved scalar at the flame front. We have

$$S(y_f) = S_f = Y_{O_\infty} \Big/ \left(Y_{O_\infty} + \frac{W_O \nu_O}{W_F \nu_F} Y_{F_{-\infty}} \right). \tag{3.29}$$

The location of the flame front can be obtained by solving

$$S(y_f) = S_f. \tag{3.30}$$

This relation divides the domain into two subdomains. The fuel side is given by $-\infty < y \leqslant y_f$ and the oxidizer side by $y_f \leqslant y < \infty$. Expressions for the temperature and species can be recovered from the relations in (3.26). On the fuel side, we have

$$T = T_{-\infty} S + \left[T_\infty + Y_{O_\infty} \frac{Q}{c_p} \frac{W_F \nu_F}{W_O \nu_O} \right] (1 - S), \tag{3.31}$$

$$Y_F = Y_{F_{-\infty}} S + Y_{O_\infty} \frac{W_F \nu_F}{W_O \nu_O} (S - 1), \tag{3.32}$$

$$Y_O = 0, \tag{3.33}$$

$$Y_P = Y_{O_\infty} \frac{W_P \nu_P}{W_O \nu_O} (1 - S), \tag{3.34}$$

and

$$Y_N = Y_{N_\infty} (1 - S) + Y_{N_{-\infty}} S. \tag{3.35}$$

On the oxidizer side, we have

$$T = T_\infty (1 - S) + \left[\frac{Q}{c_p} Y_{F_{-\infty}} + T_{-\infty} \right] S, \tag{3.36}$$

$$Y_F = 0, \tag{3.37}$$

$$Y_O = Y_{O_\infty} (1 - S) - Y_{F_{-\infty}} \frac{W_O \nu_O}{W_F \nu_F} S, \tag{3.38}$$

$$Y_P = \frac{W_P \nu_P}{W_F \nu_F} Y_{F_{-\infty}} S, \tag{3.39}$$

and

$$Y_N = Y_{N_\infty}(1-S) + Y_{N_{-\infty}} S. \tag{3.40}$$

We point out that, if we have two products, i.e.,

$$\nu_F F + \nu_O O \rightarrow \nu_{P_1} P_1 + \nu_{P_2} P_2, \tag{3.41}$$

then, since $Y_P = Y_{P_1} + Y_{P_2}$, we can recover Y_{P_1} and Y_{P_2} by forming

$$Y_{P_1} = \left(\frac{W_{P_1} \nu_{P_1}}{W_{P_1} \nu_{P_1} + W_{P_2} \nu_{P_2}} \right) Y_P, \tag{3.42}$$

and

$$Y_{P_2} = \left(\frac{W_{P_2} \nu_{P_2}}{W_{P_1} \nu_{P_1} + W_{P_2} \nu_{P_2}} \right) Y_P. \tag{3.43}$$

Combining these ideas, our flame sheet starting procedure reduces to the solution of

$$\frac{dV}{dy} + 2a\rho f' = 0, \tag{3.44}$$

$$\frac{d}{dy}\left(\mu \frac{df'}{dy} \right) - V \frac{df'}{dy} + a(\rho_\infty - \rho(f')^2) = 0, \tag{3.45}$$

$$\frac{d}{dy}\left(\rho D \frac{dS}{dy} \right) - V \frac{dS}{dy} = 0, \tag{3.46}$$

with the boundary conditions at $y = -\infty$ given by

$$V = V_{-\infty}, \tag{3.47}$$

$$f' = \sqrt{\rho_\infty / \rho_{-\infty}}, \tag{3.48}$$

$$S = 1, \tag{3.49}$$

and at $y = \infty$ by

$$f' = 1, \tag{3.50}$$

$$S = 0. \tag{3.51}$$

For a given profile of the conserved scalar, we solve (3.30) for the location of the flame front. We then utilize the relations in (3.31)–(3.40) to obtain expressions for T, Y_F, Y_O, Y_P, and Y_N. The recovered temperature profile is used in the ideal gas law to evaluate the density. The temperature is also needed to form the viscosity and the diffusion coefficients. If we introduce the Prandtl number

$$\mathrm{Pr} = \mu c_p / \lambda, \tag{3.52}$$

and recall that all of the Lewis numbers are equal to one, we can write

$$\rho D = \frac{\lambda}{c_p} = \frac{\mu}{(\mathrm{Pr})_{\mathrm{ref}}}, \tag{3.53}$$

where $(\mathrm{Pr})_{\mathrm{ref}}$ is a reference Prandtl number. Specifically, we use an approximate value for air, $(\mathrm{Pr})_{\mathrm{ref}} = 0.75$. Hence, determination of ρD is reduced to the specification of a transport relation for the viscosity. We use the simple power law

$$\mu = \mu_0 (T/T_0)^r, \tag{3.54}$$

where $r = 0.7$, $T_0 = 298\mathrm{K}$, and $\mu_0 = 1.85 \times 10^{-4}\mathrm{gm/cm\text{-}s}$ is again a reference value for air [18]. The temperature exponent was determined by fitting the equation in (3.54) to the mixture viscosity and temperature data of a representative finite rate chemistry calculation. The scaled heat release parameter $Q/c_p = \Delta T$ can be determined from an estimate of the peak temperature (e.g., from an experiment) or from the heat of combustion of the system under consideration and a representative heat capacity.

4. Numerical Results

In this section we apply the flame sheet starting estimate to two counterflow diffusion flame problems. In the first case, we model a diluted methane–air flame in the cylindrical double-jet configuration (see Fig. 1). In the second case, we consider a methane–air flame in the Tsuji geometry (see Fig. 2). The flame sheet model provides initial solution profiles for the mass flux in the transverse direction, V, the similarity function, f', the temperature, T, and the major species, i.e., CH_4, O_2, N_2, CO_2, and H_2O. The minor species were approximated by Gaussian profiles that were centered in the reaction zone and had peak heights of at most a few percent. To conserve mass in the starting estimate, the N_2 mass fraction was reduced accordingly. The detailed kinetics mechanism used in the calculations is listed in Table I (see also [19]).

Once the flame sheet starting estimate is obtained, we solve the full set of governing equations in a two-step procedure. We first determine a solution to the mass, momentum, and species equations (2.8)–(2.10) based on the flame sheet temperature profile. This fixed flame sheet temperature solution (labeled the T_{OUT} solution) is then used as input to the full fluid dynamic-thermochemistry model (2.8)–(2.11), in which the energy equation is included. The solution to the full system is labeled T_{IN}. This procedure helps to reduce both convergence difficulties and total CPU time, and is similar to the two-pass solution method used in the solution of adiabatic premixed laminar flames in [7].

Problem 1

The first problem we consider is a diluted methane–air flame in a double-jet configuration [2]. The separation distance of the jets is 1.4876 cm. The boundary conditions at the fuel jet $y = L_F = -0.6$ cm are given by

$$V = 2.8 \times 10^{-2}, \tag{4.1}$$

TABLE I

Chemical Kinetics Mechanism for the Oxidation of Methane

	Reaction	A	β	E
1.	$CH_4 + M \rightleftharpoons CH_3 + H + M$	$1.00E+17$	0.000	86000.
2.	$CH_4 + H \rightleftharpoons CH_3 + HO_2$	$7.90E+13$	0.000	56000.
3.	$CH_4 + H \rightleftharpoons CH_3 + H_2$	$2.20E+04$	3.000	8750.
4.	$CH_4 + O \rightleftharpoons CH_3 + OH$	$1.60E+06$	2.360	7400.
5.	$CH_4 + OH \rightleftharpoons CH_3 + H_2O$	$1.60E+06$	2.100	2460.
6.	$CH_2O + OH \rightleftharpoons HCO + H_2O$	$7.53E+12$	0.000	167.
7.	$CH_2O + H \rightleftharpoons HCO + H_2$	$3.31E+14$	0.000	10500.
8.	$CH_2O + M \rightleftharpoons HCO + H + M$	$3.31E+16$	0.000	81000.
9.	$CH_2O + O \rightleftharpoons HCO + OH$	$1.81E+13$	0.000	3082.
10.	$HCO + OH \rightleftharpoons CO + H_2O$	$5.00E+12$	0.000	0.
11.	$HCO + M \rightleftharpoons H + CO + M$	$1.60E+14$	0.000	14700.
12.	$HCO + H \rightleftharpoons CO + H_2$	$4.00E+13$	0.000	0.
13.	$HCO + O \rightleftharpoons OH + CO$	$1.00E+13$	0.000	0.
14.	$HCO + O_2 \rightleftharpoons HO_2 + CO$	$3.00E+12$	0.000	0.
15	$CO + O + M \rightleftharpoons CO_2 + M$	$3.20E+13$	0.000	−4200.
16.	$CO + OH \rightleftharpoons CO_2 + H$	$1.51E+07$	1.300	−758.
17.	$CO + O_2 \rightleftharpoons CO_2 + O$	$1.60E+13$	0.000	41000.
18.	$CH_3 + O_2 \rightleftharpoons CH_3O + O$	$7.00E+12$	0.000	25652.
19.	$CH_3O + M \rightleftharpoons CH_2O + H + M$	$2.40E+13$	0.000	28812.
20.	$CH_3O + H \rightleftharpoons CH_2O + H_2$	$2.00E+13$	0.000	0.
21.	$CH_3O + OH \rightleftharpoons CH_2O + H_2O$	$1.00E+13$	0.000	0.
22.	$CH_3O + O \rightleftharpoons CH_2O + OH$	$1.00E+13$	0.000	0.
23.	$CH_3O + O_2 \rightleftharpoons CH_2O + HO_2$	$6.30E+10$	0.000	2600.
24.	$CH_3 + O_2 \rightleftharpoons CH_2O + OH$	$5.20E+13$	0.000	34574.
25.	$CH_3 + O \rightleftharpoons CH_2O + H$	$6.80E+13$	0.000	0.
26.	$CH_3 + OH \rightleftharpoons CH_2O + H_2$	$7.50E+12$	0.000	0.
27	$HO_2 + CO \rightleftharpoons CO_2 + OH$	$5.80E+13$	0.000	22934.
28.	$H_2 + O_2 \rightleftharpoons 2OH$	$1.70E+13$	0.000	47780.
29.	$OH + H_2 \rightleftharpoons H_2O + H$	$1.17E+09$	1.300	3626.
30.	$H + O_2 \rightleftharpoons OH + O$	$2.20E+14$	0.000	16800.
31.	$O + H_2 \rightleftharpoons OH + H$	$1.80E+10$	1.000	8826.
32.	$H + O_2 + M \rightleftharpoons HO_2 + M^a$	$2.10E+18$	−1.000	0.
33.	$H + O_2 + O_2 \rightleftharpoons HO_2 + O_2$	$6.70E+19$	−1.420	0.
34.	$H + O_2 + N_2 \rightleftharpoons HO_2 + N_2$	$6.70E+19$	−1.420	0.
35.	$OH + HO_2 \rightleftharpoons H_2O + O_2$	$5.00E+13$	0.000	1000.
36.	$H + HO_2 \rightleftharpoons 2OH$	$2.50E+14$	0.000	1900.
37.	$O + HO_2 \rightleftharpoons O_2 + OH$	$4.80E+13$	0.000	1000.
38.	$2OH \rightleftharpoons O + H_2O$	$6.00E+08$	1.300	0.
39.	$H_2 + M \rightleftharpoons H + H + M^b$	$2.23E+12$	0.500	92600.
40.	$O_2 + M \rightleftharpoons O + O + M$	$1.85E+11$	0.500	95560.
41.	$H + OH + M \rightleftharpoons H_2O + M^c$	$7.50E+23$	−2.600	0.
42.	$H + HO_2 \rightleftharpoons H_2 + O_2$	$2.50E+13$	0.000	700.
43.	$HO_2 + HO_2 \rightleftharpoons H_2O_2 + O_2$	$2.00E+12$	0.000	0.
44.	$H_2O_2 + M \rightleftharpoons OH + OH + M$	$1.30E+17$	0.000	45500.
45.	$H_2O_2 + H \rightleftharpoons HO_2 + H_2$	$1.60E+12$	0.000	3800.
46.	$H_2O_2 + OH \rightleftharpoons H_2O + HO_2$	$1.00E+13$	0.000	1800.

Note. Reaction mechanism rate coefficients in the form $k_f = AT^\beta \exp(-E_0/RT)$. Units are moles, cubic centimeters, seconds, Kelvins and calories/mole.

[a] Third body efficiencies: $k_{32}(H_2O) = 21k_{32}(Ar)$, $k_{32}(H_2) = 3.3k_{32}(Ar)$, $k_{32}(N_2) = k_{32}(O_2) = 0$.

[b] Third body efficiencies: $k_{39}(H_2O) = 6k_{39}(Ar)$, $k_{39}(H) = 2k_{39}(Ar)$, $k_{39}(H_2) = 3k_{39}(Ar)$.

[c] Third body efficiency: $k_{41}(H_2O) = 20k_{41}(Ar)$.

$$f' = 1.216, \tag{4.2}$$

$$Y_{CH_4} = 0.598, \qquad Y_{N_2} = 0.402, \qquad Y_{k \neq CH_4, N_2} = 0, \tag{4.3}$$

$$T = 294\text{K}, \tag{4.4}$$

and at the oxidizer jet $y = L_{OX} = 0.8876$ cm by

$$f' = 1.0, \tag{4.5}$$

$$Y_{O_2} = 0.18, \qquad Y_{N_2} = 0.82, \qquad Y_{k \neq O_2, N_2} = 0, \tag{4.6}$$

$$T = 294\text{K}. \tag{4.7}$$

The mass flow rate is in units of gm/cm^2-s and the densities of the fuel and the oxidizer mixtures were used in obtaining the value of the similarity function at the fuel jet. The mass flow rate boundary condition corresponds to a fuel duct velocity of 35 cm/s. The strain rate used in the calculation was $a = 40\text{s}^{-1}$.

An adaptive two-point boundary value solver (see [6]) was used to generate the flame sheet starting estimate. A solution was obtained on a nonuniform grid consisting of 38 grid points. This solution was then used as the starting estimate for the fixed temperature solution. One hundred adaptive time steps were taken to help bring the solution within the domain of convergence of Newton's method on the 38-point grid. After the time steps, Newton's method converged with only one iteration. Once this solution was obtained, the mesh was refined and a solution was calculated on the finer grid. This procedure continued until the adaptive mesh

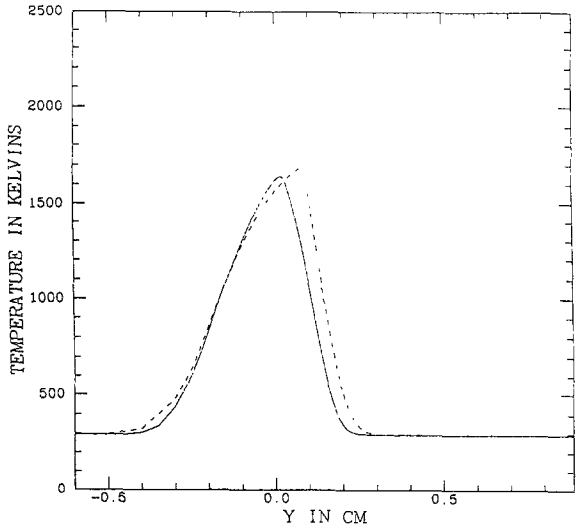

FIG. 3. Comparison between the calculated flame sheet temperature profile (dotted line) and the calculated finite rate chemistry temperature profile (solid line) in the double-jet problem.

criteria were satisfied (see, e.g., [6]). The refined fixed-temperature solution was then used as the starting estimate for the complete fluid dynamic-thermochemistry solution. Two additional grid refinements were performed to obtain a final solution on a grid consisting of 65 nonuniform points. On the refined grids Newton's method converged with only 10–20 additional time steps. The mesh spacing was such that 600 equispaced points would have been needed to obtain comparable accuracy. The total CPU time for the entire procedure was approximately 3h 40 min on a VAX-8600. Approximately 6 CPU seconds were needed for the flame sheet calculation, 130 min for the T_{OUT} calculation and approximately 90 min for the T_{IN} solution. We were unable to obtain a complete T_{IN} solution for this problem when the procedure previously used for premixed laminar flames was for the temperature, the similarity function and the normal velocity followed.

In Fig. 3–5 we compare the flame sheet profiles with the calculated finite rate profiles. We observe that the flame sheet solution predicts all of the qualitative features of the detailed kinetics temperature, similarity function, and normal velocity solutions, especially the relative locations of the temperature peak, the stagnation point, and the "double peak" velocity profile. In Fig. 6–8 profiles for the major and minor species are illustrated for the detailed kinetics solution. The convenient hypotheses of an infinitesimally thin flame zone, a globally uniform heat capacity, and the simple diffusion laws (3.52)–(3.54), along with the coarseness of the flame sheet solution mesh all contribute to the observed differences in the profiles of the two models. Some of the "errors" of the flame sheet model have a self-cancelling tendency; for instance, the characteristic cusp of the thin flame is broadened by being represented on a coarse grid. A posteriori refinements to bring

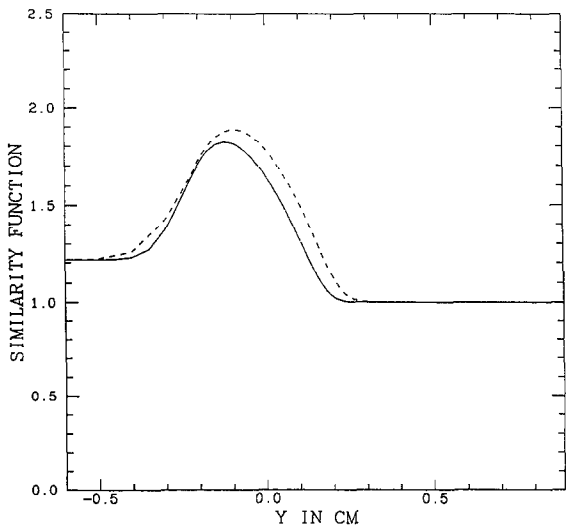

FIG. 4. Comparison between the calculated flame sheet similarity function profile (dotted line) and the calculated finite rate chemistry similarity function profile (solid line) in the double-jet problem.

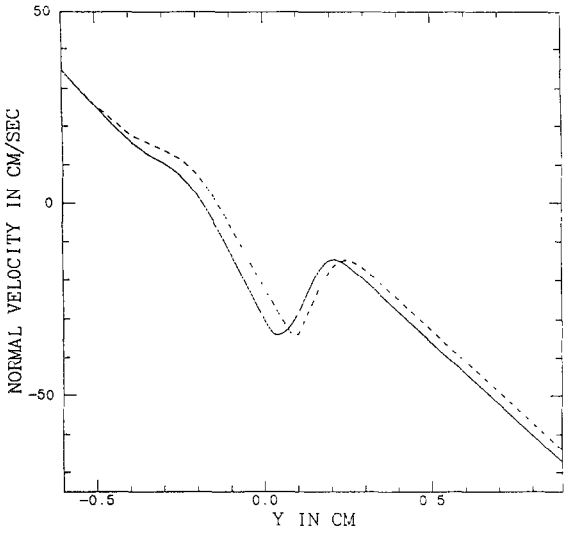

FIG. 5. Comparison between the calculated flame sheet normal velocity profile (dotted line) and the calculated finite rate chemistry normal velocity profile (solid line) in the double-jet problem.

the flame sheet model into further conformity with the detailed kinetics solution are possible. For instance, c_p can be adjusted to yield the proper peak temperature and varying the exponent r in (3.54) has a tendency to move the diffusion-controlled flame laterally. However, such refinements are not relevant to our computational modeling program, since possession of the detailed kinetics profile renders further use of the flame sheet unnecessary. A flame sheet model which provides profiles

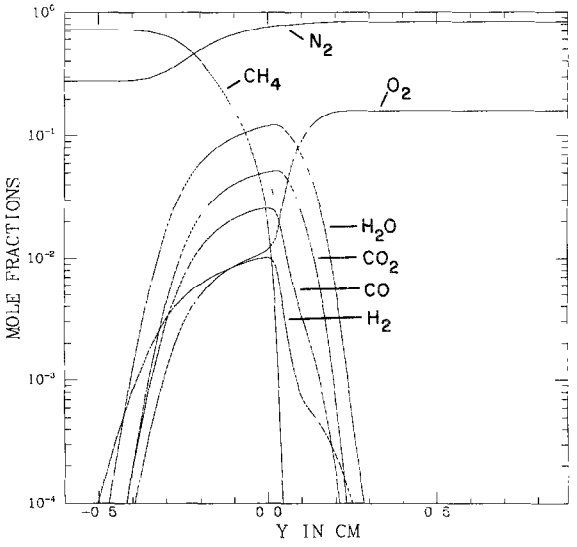

FIG. 6. Calculated finite rate chemistry profiles of the major species in the double-jet flame.

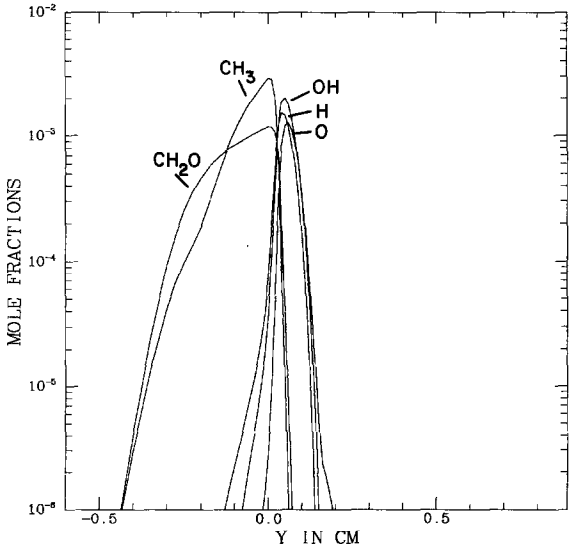

FIG. 7. Calculated finite rate chemistry profiles of the minor species and radicals in the double-jet flame.

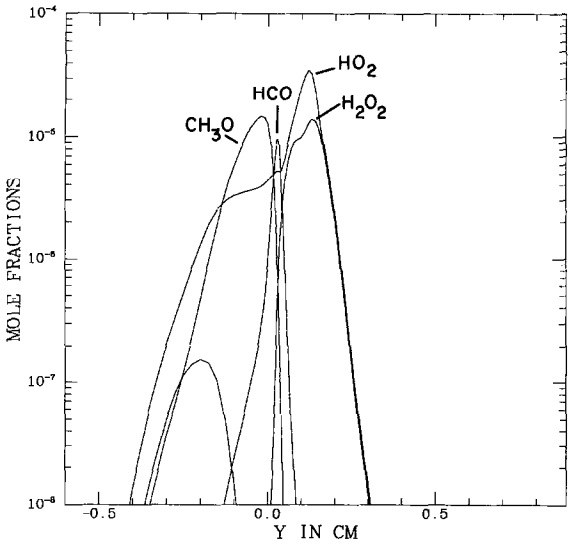

FIG. 8. Calculated finite rate chemistry profiles of the trace reacting species and radicals in the double-jet flame.

from which our time-stepping/Newton's method boundary value problem solver will converge is sufficiently "correct."

The detailed species profiles in Fig. 6–8 are dependent on the choice of reaction mechanism (particularly for the minor species), and the feedback they provide is of use to kineticists in ascertaining the importance of various components of the overall mechanism. It is interesting to interpret the results contained in Fig. 7, for instance, in light of the recent work of Westbrook and Dryer [20]. They have postulated that the oxidation of methane occurs through roughly two parallel paths. One path consists of direct oxidation of methyl radicals to methoxy radicals and/or formaldehyde and in the the second path methyl radical recombination is followed by the oxidation of the resulting C_2 species. In our calculations, the former path was chosen and the latter path was neglected. Hence, in Fig. 7 we illustrate CH_3 and CH_2O concentrations on the rich side of the reaction zone. Figure 7 also illustrates that the peak values of the radicals H, O, and OH are observed on the lean side of the flame and their concentration is small at the reaction zone. This is due to the high affinity of CH_4 to the radicals H, O, and OH which causes their concentration to increase only after the concentration of CH_4 has reached a small value. As a result, the oxidation of CO and H_2 occurs predominantly on the lean side of the reaction zone.

Problem 2

The second problem we consider is a methane–air flame in the Tsuji configuration. This problem has been studied by Dixon-Lewis *et al.* [8] (see also,

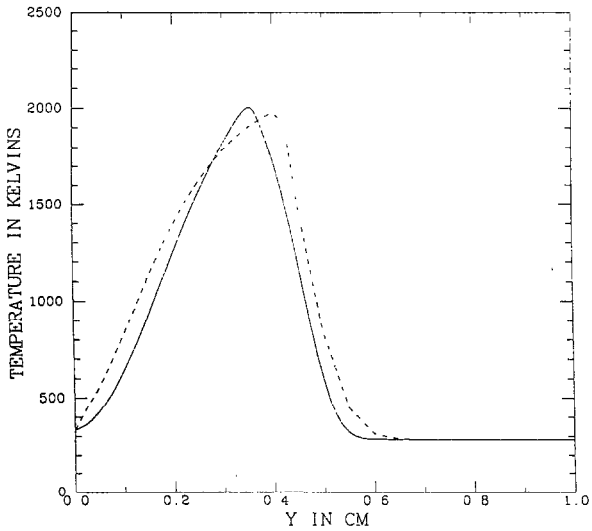

FIG. 9. Comparison between the calculated flame sheet temperature profile (dotted line) and the calculated finite rate chemistry temperature profile (solid line) for the Tsuji configuration.

[19]). We use a computational domain of 1.0 cm and a strain rate of $a = 100\text{s}^{-1}$. The boundary conditions at the cylinder surface $y = 0$ are given by

$$V = 7.068 \times 10^{-3}, \tag{4.8}$$

$$f' = 0, \tag{4.9}$$

$$Y_{CH_4} = 1.0, \qquad Y_{k \neq CH_4} = 0, \tag{4.10}$$

$$T = 332.16\ \text{K}, \tag{4.11}$$

and at $y = 1.0$ cm by

$$f' = 1.0, \tag{4.12}$$

$$Y_{O_2} = 0.233, \qquad Y_{N_2} = 0.767, \qquad Y_{k \neq O_2, N_2} = 0, \tag{4.13}$$

$$T = 283.16\ \text{K}. \tag{4.14}$$

The mass flow rate boundary condition corresponds to a fuel velocity of 12.04 cm/s.

The solution procedure was identical to that used in the double-jet problem. The flame sheet equations were solved first on a nonuniform grid consisting of 31 points. This solution was then used as the starting estimate for the fixed temperature calculation. Once a refined, fixed temperature solution was obtained, the full fluid dynamic-thermochemistry solution was calculated. A total of 3 grid refinements were used in generating a solution on a nonuniform grid consisting of 70 points. As many as 267 equispaced points would have been needed to obtain comparable accuracy.

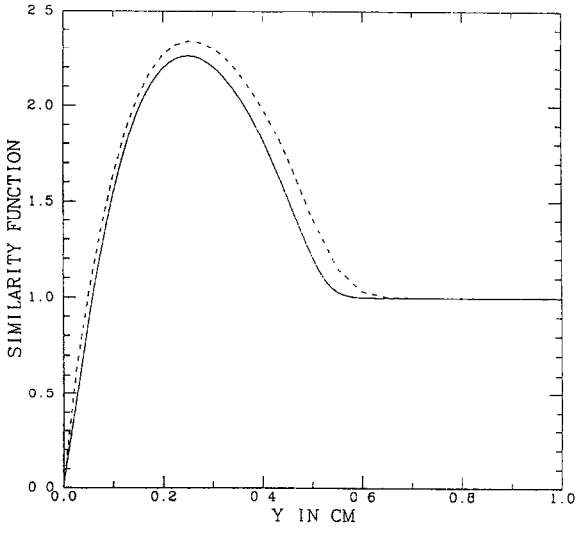

FIG. 10. Comparison between the calculated flame sheet similarity function profile (dotted line) and the calculated finite rate chemistry similarity function profile (solid line) for the Tsuji configuration.

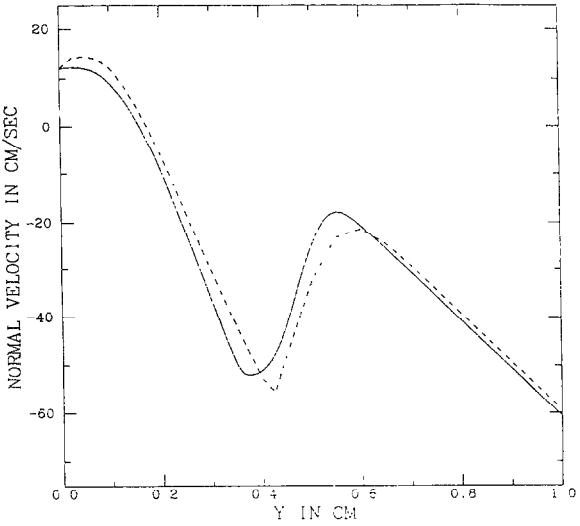

FIG. 11. Comparison between the calculated flame sheet normal velocity profile (dotted line) and the calculated finite rate chemistry normal velocity profile (solid line) for the Tsuji configuration.

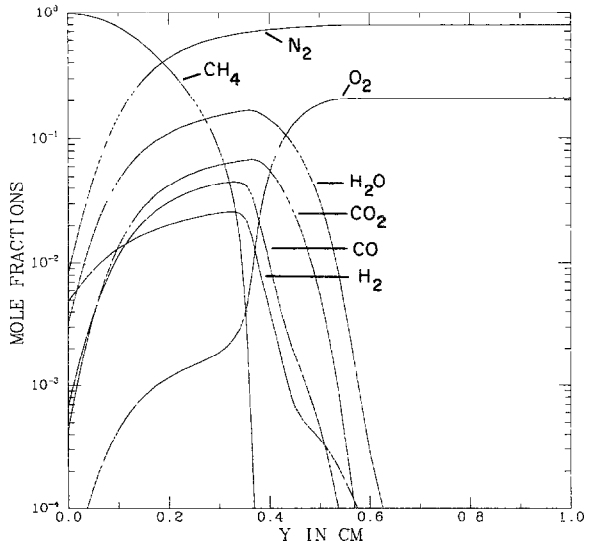

FIG. 12. Calculated finite rate chemistry profiles of the major species in the Tsuji flame.

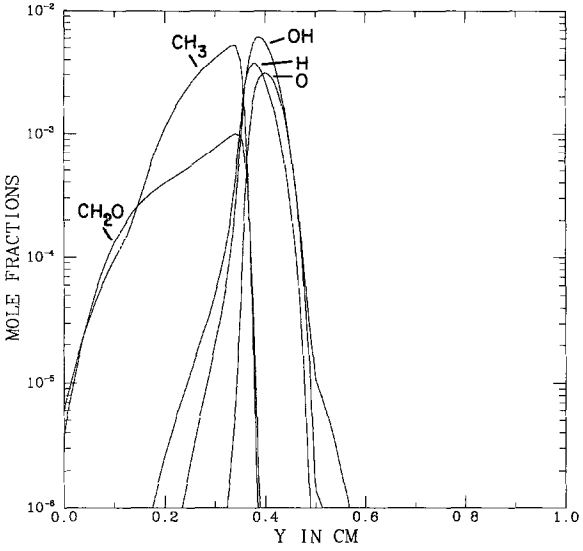

FIG. 13. Calculated finite rate chemistry profiles of the minor species and radicals in the Tsuji flame.

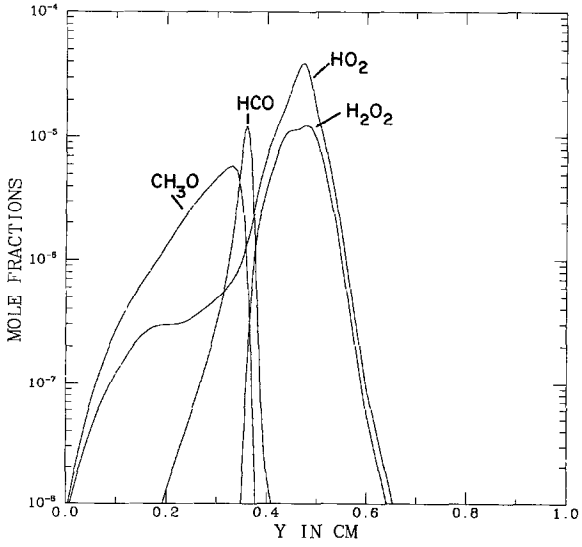

FIG. 14. Calculated finite rate chemistry profiles of the trace reacting species and radicals in the Tsuji flame.

The number of time steps and complete Newton iterations were comparable to the statistics of Problem 1. Approximately 6 seconds of CPU time were needed to generate the flame sheet calculation with 140 min for the T_{OUT} solution and 85 min for the T_{IN} solution. We point out that in a previous calculation (see, e.g., [19]) we were able to obtain a T_{IN} solution when the initial temperature profile was obtained from a constant enthalpy-constant pressure equilibrium calculation. Using the flame sheet starting estimates, however, we were able to generate a T_{IN} solution with approximately one-tenth of the CPU time required for the constant enthalpy-constant pressure T_{IN} calculation. Results similar to those contained in Fig. 3–8 are illustrated in Fig. 9–14. We again observe that agreement is generally quite good for the temperature, the similarity function, and the normal velocity component.

5. Conclusions

In this paper we have developed a flame sheet starting procedure for laminar counterflow diffusion flame problems. The model couples the equations of mass and tangential momentum with a Shvab–Zeldovich equation to provide estimates for the mass flux in the transverse direction, the similarity function, the temperature, and the stable major species in the flame. The procedure is formulated for both the porous cylinder (Tsuji) and the cylindrical double-jet (Seshadri) configurations. Application of the model to two laboratory methane–air flames reveals the effectiveness of the procedure in generating starting estimates for such problems.

References

1. N. Peters, *Prog. Energy Combust. Sci.* **10**, 319 (1984).
2. I. K. Puri and K. Seshadri, *Combust. Flame* **65**, 137 (1986).
3. H. Tsuji and I. Yamaoka, *Twelfth Symposium (International) on Combustion, The Combustion Institute*, 1969, p. 997.
4. H. Tsuji and I. Yamaoka, *Thirteenth Symposium (International) on Combustion, The Combustion Institute*, 1971, p. 723.
5. H. Tsuji, *Prog. Energy Combust. Sci.* **8**, 93 (1982).
6. M. D. Smooke, *J. Comput. Phys.* **48**, 72 (1982).
7. M. D. Smooke, J. A. Miller, and R. J. Kee, *Combust. Sci. Technol.* **34**, 79 (1983).
8. G. Dixon-Lewis, T. David, P. H. Gaskell, S. Fukutani, H. Jinno, J. A. Miller, R. J. Kee, M. D. Smooke, N. Peters, E. Effelsberg, J. Warnatz, and F. Behrendt, *Twentieth Symposium (International) on Combustion, The Combustion Institute*, 1985, p. 1893.
9. R. J. Kee, J. A. Miller, and T. H. Jefferson, Sandia National Laboratories Report SAND 80-8003, 1980.
10. R. J. Kee, J. Warnatz, and J. A. Miller, Sandia National Laboratories Report SAND 83-8209, 1983.
11. J. A. Miller, M. D. Smooke, R. M. Green, and R. J. Kee, *Combust. Sci. Technol.* **34**, 149 (1983).
12. J. A. Miller, R. E. Mitchell, M. D. Smooke, and R. J. Kee, *Nineteenth Symposium (International) on Combustion, The Combustion Institute*, 1981, p. 181.
13. S. P. Burke and T. E. W. Schumann, *Ind. Eng. Chem.* **29**, 998 (1928).

14. H. W. SMITH, R. A. SCHMITZ, AND R. G. LADD, *Combust. Sci. Technol.* **4**, 131 (1971).
15. R. E. MITCHELL, Sc. D. thesis, MIT, 1975.
16. R. E. MITCHELL, A. F. SAROFIM, AND L. A. CLOMBURG, *Combust. Flame* **37**, 227 (1980).
17. F. A. WILLIAMS, *Combustion Theory* (Addison–Wesley, Reading, MA, 1965).
18. A. M. KANURY, *Combustion Phenomena* (Gordon & Breach, New York, 1982).
19. J. A. MILLER, R. J. KEE, M. D. SMOOKE, AND J. F. GRCAR, in 1984 *Spring Meeting of the Western States Section of the Combustion Institute, University of Colorado, Boulder*, 1984.
20. C. K. WESTBROOK AND F. L. DRYER, *Prog. Energy Combust. Sci.* **10**, 1 (1984).